

LSNN METHOD FOR SCALAR NONLINEAR HCLS: DISCRETE DIVERGENCE OPERATOR*

ZHIQIANG CAI[†], JINGSHUANG CHEN[†], AND MIN LIU[‡]

Abstract. The least-squares neural network (LSNN) method was introduced for solving scalar linear and nonlinear hyperbolic conservation laws in [6, 5]. The method is based on an equivalent least-squares (LS) formulation and employs ReLU neural network as approximating functions, that is especially suitable for approximating discontinuous functions with unknown interface location. In design of the LSNN method for HCLS, numerical approximation of differential operator plays a critical role, and standard numerical or automatic differentiation along coordinate directions usually results in a failing NN-based method. To overcome this difficulty, this paper rewrites HCLS in their divergence form of space and time and introduces a new discrete divergence operator.

Theoretically, accuracy of the discrete divergence operator is estimated even if the solution is discontinuous. Numerically, the resulting LSNN method with the new discrete divergence operator is tested for several benchmark problems with both convex and non-convex fluxes; the method is capable of computing the correct physical solution for problems with rarefaction waves and capturing the shock of the underlying problem without oscillation or smearing.

Key words. discrete divergence operator, least-squares method, ReLU neural network, scalar nonlinear hyperbolic conservation law

AMS subject classifications.

1. Introduction. Numerical approximations to solutions of nonlinear hyperbolic conservation laws (HCLS) are computationally challenging. Partly, this is due to the fact that solutions of HCLS are discontinuous at unknown locations, which poses a great difficulty in approximation when using fixed, quasi-uniform meshes. Many advanced numerical methods have been developed to address this issue during the past five decades (see, e.g., [29, 31, 30, 15, 18, 19, 24] for higher order finite volume/difference methods using limiters, filters, ENO/WENO, etc. and [9, 3, 10, 13, 4, 20, 21] for discontinuous and/or adaptive finite element methods).

Neural networks (NNs) as a new class of approximating functions have been used recently for solving partial differential equations (see, e.g., [8, 28, 32]) due to their expressive power. A special feature of NNs is their free hyper-planes implicitly generated by neurons that can automatically adapt to the target function and the solution of a PDE. In other words, ReLU NN generates continuous piece-wise linear functions on irregular free/moving meshes, and hence does not suffer standard approximation deficiencies on fixed meshes. This property of NNs was used in [6] for solving linear advection-reaction problem with discontinuous solution without using information on location of discontinuous interfaces. Specifically, the least-squares NN method studied in [6] is based on the least-squares formulation studied in ([2, 11]), uses ReLU NNs as approximating functions, and approximates the differential operator by directional numerical differentiation. Compared to various AMR methods that locate discontinuous interfaces through adaptive mesh refinement process, the LSNN method is much more effective in terms of the number of degrees of freedom (DoF).

For nonlinear hyperbolic conservation laws, solutions are often discontinuous due to shock formation, and it is well-known that the differential form of a HCL is invalid at discontinuous interface (where solution is discontinuous). This implies that the directional numerical differentiation of the differential operator based on the differential form used in [6] is not applicable to nonlinear HCLS. To circumvent this obstacle, one needs to use the integral form of the HCLS (see, e.g., [24]), that

*This work was supported in part by the National Science Foundation under grant DMS-2110571.

[†]Department of Mathematics, Purdue University, 150 N. University Street, West Lafayette, IN 47907-2067 (caiz@purdue.edu, chen2042@purdue.edu).

[‡]School of Mechanical Engineering, Purdue University, 585 Purdue Mall, West Lafayette, IN 47907-2088(liu66@purdue.edu).

is valid for problems having discontinuous solutions, at least at the discontinuous interface. This explains why the integral form is the foundation of all conservative methods such as Roe’s scheme [29], ENO [17], WENO [30, 31], etc.

By employing the Roe and ENO fluxes to approximate the divergence operator, in [5] we tested the resulting LSNN method for scalar nonlinear HCLs. Numerical results for the inviscid Burgers equation showed that the LSNN method with conservative numerical differentiation is capable of capturing the shock without smearing and oscillation. Moreover, the LSNN method has much less DoF than traditional mesh-based methods.

Despite the promising results obtained in [5], we also observed some limitations of the LSNN method when using conservative numerical differentiation of the Roe and second-order ENO fluxes. For example, the resulting LSNN method is not accurate for complicated initial condition, and it also has issues for problems with rarefaction waves and with non-convex spatial fluxes. To improve accuracy of the LSNN method, an obvious choice on conservative numerical differentiation is to adopt existing “higher order” conservative methods such as ENO, WENO, etc. However, those conservative schemes are based on time evolution and were developed in the setting of traditional mesh-based methods; moreover, the “higher order” here is measured for smooth solutions.

In this paper, we develop a new discrete divergence operator that is an accurate approximation to the divergence operator even if the solution is discontinuous. Specifically, the new discrete divergence operator at center of a control volume is defined as an approximation to the average value of the divergence operator over the control volume; the average value is then represented by surface integral through the Gauss divergence theorem; finally the surface integral is approximated by the *composite* mid-point/trapezoidal numerical integration. By using enough surface integration points, we show theoretically that the resulting discrete divergence operator is as accurate as we desire (see Lemma 4.3 and Remark 4.4) even if the solution is discontinuous. The reason that all points on the surface are at our disposal for numerical integration is because the LSNN is a “mesh/point-less” space-time method.

Theoretically, we show that the residual of the LSNN approximation using newly developed discrete divergence operator is bounded by the best approximation of the class of NN functions in some measure (see Lemma 3.1) plus the approximation error of numerical integration and differentiation (see Lemma 3.3). Numerically, for the inviscid Burgers equation with various initial conditions, we show that the LSNN method using new discrete divergence operator is able to compute the right physical solution and to capture shock without oscillation or smearing, and is much more accurate than the LSNN method in [5]. Moreover, the LSNN method using new discrete divergence operator works well for the problem with non-convex flux or rarefaction waves.

The paper is organized as follows. Section 2 describes the hyperbolic conservation law, its least-squares formulation, and preliminaries. The space-time LSNN method and its block version are presented in Sections 3. The discrete divergence operator and its error bound is introduced and analyzed in Section 4. Finally, numerical results for various benchmark test problems are given in Section 5.

2. Problem Formulation. Let $\tilde{\Omega}$ be a bounded domain in \mathbb{R}^d ($d = 1, 2, \text{ or } 3$) with Lipschitz boundary, and $I = (0, T)$ be the temporal interval. Consider the scalar nonlinear hyperbolic conservation law

$$(2.1) \quad \begin{cases} u_t(\mathbf{x}, t) + \nabla_{\mathbf{x}} \cdot \tilde{\mathbf{f}}(u) = 0, & \text{in } \tilde{\Omega} \times I, \\ u = \tilde{g}, & \text{on } \tilde{\Gamma}_-, \\ u(\mathbf{x}, 0) = u_0(\mathbf{x}), & \text{in } \tilde{\Omega}, \end{cases}$$

where u_t is the partial derivative of u with respect to the temporal variable t ; $\nabla_{\mathbf{x}} \cdot$ is a divergence operator with respect to the spatial variable \mathbf{x} ; $\tilde{\mathbf{f}}(u) = (f_1(u), \dots, f_d(u))$ is the spatial flux vector field; $\tilde{\Gamma}_-$ is the part of the boundary $\partial\tilde{\Omega} \times I$ where the characteristic curves enter the domain $\tilde{\Omega} \times I$;

and the boundary data \tilde{g} and the initial data u_0 are given scalar-valued functions. Without loss of generality, assume that $f_i(u)$ is twice differentiable for $i = 1, \dots, d$.

Problem (2.1) is a hyperbolic partial differential equation defined on a space-time domain $\Omega = \tilde{\Omega} \times I$ in \mathbb{R}^{d+1} . Denote the inflow boundary of the domain Ω and the inflow boundary condition by

$$\Gamma_- = \begin{cases} \tilde{\Gamma}_-, & t \in (0, T), \\ \Omega, & t = 0 \end{cases} \quad \text{and} \quad g = \begin{cases} \tilde{g}, & \text{on } \tilde{\Gamma}_-, \\ u_0(\mathbf{x}), & \text{on } \Omega, \end{cases}$$

respectively. Then (2.1) may be rewritten as the following compact form

$$(2.2) \quad \begin{cases} \mathbf{div} \mathbf{f}(u) = 0, & \text{in } \Omega \in \mathbb{R}^{d+1}, \\ u = g, & \text{on } \Gamma_-, \end{cases}$$

where $\mathbf{div} = (\partial_{x_1}, \dots, \partial_{x_d}, \partial_t)$ is a divergence operator with respect to both spatial and temporal variables $\mathbf{z} = (\mathbf{x}, t)$, and $\mathbf{f}(u) = (f_1(u), \dots, f_d(u), u) = (\hat{\mathbf{f}}(u), u)$ is the spatial and temporal flux vector field. Assume that $u \in L^\infty(\Omega)$. Then u is called a weak solution of (2.2) if and only if

$$(2.3) \quad -(\mathbf{f}(u), \nabla \varphi)_{0, \Omega} + (\mathbf{n} \cdot \mathbf{f}(u), \varphi)_{0, \Gamma_-} = 0, \quad \forall \varphi \in C_{\Gamma_+}^1(\bar{\omega}),$$

where $\Gamma_+ = \partial\Omega \setminus \Gamma_-$ is the outflow boundary and $C_{\Gamma_+}^1(\bar{\omega}) = \{\varphi \in C^1(\bar{\omega}) : \varphi = 0 \text{ on } \Gamma_+\}$.

Denote the collection of square integrable vector fields whose divergence is also square integrable by

$$H(\text{div}; \Omega) = \{\boldsymbol{\tau} \in L^2(\Omega)^{d+1} \mid \mathbf{div} \boldsymbol{\tau} \in L^2(\Omega)\}.$$

It is then easy to see that solutions of (2.2) are in the following subset of $L^2(\Omega)$

$$(2.4) \quad \mathcal{V}_{\mathbf{f}} = \{v \in L^2(\Omega) \mid \mathbf{f}(v) \in H(\text{div}; \Omega)\}.$$

Define the least-squares (LS) functional

$$(2.5) \quad \mathcal{L}(v; g) = \|\mathbf{div} \mathbf{f}(v)\|_{0, \Omega}^2 + \|v - g\|_{0, \Gamma_-}^2,$$

where $\|\cdot\|_{0, S}$ denotes the standard $L^2(S)$ norm for $S = \Omega$ and Γ_- . Now, the corresponding least-squares formulation is to seek $u \in \mathcal{V}_{\mathbf{f}}$ such that

$$(2.6) \quad \mathcal{L}(u; g) = \min_{v \in \mathcal{V}_{\mathbf{f}}} \mathcal{L}(v; g).$$

PROPOSITION 2.1. *Assume that $u \in L^\infty(\Omega)$ is a piece-wise C^1 function. Then u is a weak solution of (2.2) if and only if u is a solution of the minimization problem in (2.6).*

Proof. The proposition is a direct consequence of Theorem 2.5 in [12]. \square

3. Least-Squares Neural Network Method. Based on the least-squares formulation in (2.6), in this section we first describe the least-squares neural network (LSNN) method for the scalar nonlinear hyperbolic conservation law and then estimate upper bound of the LSNN approximation.

To this end, denote a scalar-valued function generated by a l -layer fully connected neural network by

$$(3.1) \quad \mathcal{N}(\mathbf{z}) = \boldsymbol{\omega}^{(l)} \left(N^{(l-1)} \circ \dots \circ N^{(2)} \circ N^{(1)}(\mathbf{z}) \right) - b^{(l)} : \mathbf{z} = (\mathbf{x}, t) \in \mathbb{R}^{d+1} \longrightarrow \mathbb{R},$$

where $\boldsymbol{\omega}^{(l)} \in \mathbb{R}^{n_{l-1}}$, $b^{(l)} \in \mathbb{R}$, and the symbol \circ denotes the composition of functions. For $k = 1, \dots, l-1$, the $N^{(k)} : \mathbb{R}^{n_{k-1}} \rightarrow \mathbb{R}^{n_k}$ is called the k^{th} hidden layer of the network defined as follows:

$$(3.2) \quad N^{(k)}(\mathbf{z}^{(k-1)}) = \boldsymbol{\tau}(\boldsymbol{\omega}^{(k)} \mathbf{z}^{(k-1)} - \mathbf{b}^{(k)}) \quad \text{for } \mathbf{z}^{(k-1)} \in \mathbb{R}^{n_{k-1}},$$

where $\boldsymbol{\omega}^{(k)} \in \mathbb{R}^{n_k \times n_{k-1}}$, $\mathbf{b}^{(k)} \in \mathbb{R}^{n_k}$, $\mathbf{z}^{(0)} = \mathbf{z}$, and $\tau(s)$ is the activation function whose application to a vector is defined component-wisely. In this paper, we will use the rectified linear unit (ReLU) activation function given by

$$(3.3) \quad \tau(s) = \max\{0, s\} = \begin{cases} 0, & \text{if } s \leq 0, \\ s, & \text{if } s > 0. \end{cases}$$

As shown in [6], the ReLU is a desired activation function for approximating discontinuous solution.

Denote the set of neural network functions by

$$\mathcal{M}_N = \mathcal{M}_N(l) = \{\mathcal{N}(\mathbf{z}) \text{ defined in (3.1)} : \boldsymbol{\omega}^{(k)} \in \mathbb{R}^{n_k \times n_{k-1}}, \mathbf{b}^{(k)} \in \mathbb{R}^{n_k} \text{ for } k = 1, \dots, l\},$$

where the subscript N denotes the total number of parameters $\boldsymbol{\theta} = \{\boldsymbol{\omega}^{(k)}, \mathbf{b}^{(k)}\}$ given by

$$N = M_d(l) = \sum_{k=1}^l n_k \times (n_{k-1} + 1).$$

Obviously, the continuity of the activation function $\tau(s)$ implies that \mathcal{M}_N is a subset of $C^0(\Omega)$. Together with the smoothness assumption on spatial flux $\tilde{\mathbf{f}}(u)$, it is easy to see that \mathcal{M}_N is also a subset of $\mathcal{V}_{\mathbf{f}}$ defined in (2.4).

Since \mathcal{M}_N is not a linear subspace, it is then natural to discretize the HCL using a least-squares minimization formulation. Before defining the computationally feasible least-squares neural network (LSNN) method, let us first consider an intermediate least-squares neural network approximation: finding $u^N(\mathbf{z}; \boldsymbol{\theta}^*) \in \mathcal{M}_N$ such that

$$(3.4) \quad \mathcal{L}(u^N(\cdot; \boldsymbol{\theta}^*); g) = \min_{v \in \mathcal{M}_N} \mathcal{L}(v(\cdot; \boldsymbol{\theta}); g) = \min_{\boldsymbol{\theta} \in \mathbb{R}^N} \mathcal{L}(v(\cdot; \boldsymbol{\theta}); g).$$

LEMMA 3.1. *Let u be the solution of (2.2), and let $u^N \in \mathcal{M}_N$ be a solution of (3.4). Assume that \mathbf{f} is twice differentiable, then there exists a positive constant C such that*

$$(3.5) \quad \begin{aligned} \mathcal{L}(u^N; g) &= \inf_{v \in \mathcal{M}_N} \left(\|v - u\|_{0, \Gamma_-}^2 + \|\mathbf{div} [\mathbf{f}(v) - \mathbf{f}(u)]\|_{0, \Omega}^2 \right) \\ &\leq C \inf_{v \in \mathcal{M}_N} \left(\|v - u\|_{0, \Gamma_-}^2 + \|\mathbf{div} [\mathbf{f}'(u)(v - u)]\|_{0, \Omega}^2 \right) + h.o.t., \end{aligned}$$

where *h.o.t.* means a higher order term comparing to the first term.

Proof. For any $v \in \mathcal{M}_N$, (3.4) and (2.2) imply that

$$\mathcal{L}(u^N; g) \leq \mathcal{L}(v; g) = \|v - u\|_{0, \Gamma_-}^2 + \|\mathbf{div} [\mathbf{f}(v) - \mathbf{f}(u)]\|_{0, \Omega}^2,$$

which proves the validity of the equality in (3.5). By the Taylor expansion, there exists $\{w_i\}_{i=1}^d$ between u and v such that

$$\mathbf{f}(v) - \mathbf{f}(u) = \mathbf{f}'(u)(v - u) + \frac{1}{2} \mathbf{f}''(w)(v - u)^2,$$

where $\mathbf{f}'(u) = (f'_1(u), \dots, f'_d(u), 1)^t$ and $\mathbf{f}''(w) = (f''_1(w_1), \dots, f''_d(w_d), 0)^t$. Together with the triangle inequality we have

$$(3.6) \quad \|\mathbf{div} [\mathbf{f}(v) - \mathbf{f}(u)]\|_{0, \Omega} \leq \|\mathbf{div} [\mathbf{f}'(u)(v - u)]\|_{0, \Omega} + \frac{1}{2} \|\mathbf{div} [\mathbf{f}''(w)(v - u)^2]\|_{0, \Omega}.$$

Notice that the second term in the right-hand side of (3.6) is a higher order term comparing to the first term. Now, the inequality in (3.5) is a direct consequence of the equality in (3.5) and (3.6). This completes the proof of the lemma. \square

REMARK 3.2. When u is sufficiently smooth, the second term

$$\mathbf{div} [\mathbf{f}'(u)(v - u)] = (v - u) \mathbf{div} \mathbf{f}'(u) + \mathbf{f}'(u) \cdot \nabla(v - u)$$

may be bounded by the sum of the L^2 norms of $v - u$ and the directional derivative of $v - u$ along the direction $\mathbf{f}'(u)$.

Evaluation of the least-squares functional $\mathcal{L}(v; g)$ defined in (2.5) requires integration and differentiation over the computational domain and the inflow boundary. As in [8], we evaluate the integral of the least-squares functional by numerical integration. To do so, let

$$\mathcal{T} = \{K : K \text{ is an open subdomain of } \Omega\} \quad \text{and} \quad \mathcal{E}_- = \{E = \partial K \cap \Gamma_- : K \in \mathcal{T}\}$$

be partitions of the domain Ω and the inflow boundary Γ_- , respectively. Let $\mathbf{z}_K = (\mathbf{x}_K, t_K)$ and $\mathbf{z}_E = (\mathbf{x}_E, t_E)$ be the respective centroids of $K \in \mathcal{T}$ and $E \in \mathcal{E}_-$. The corresponding discrete least-squares functional is defined by

$$(3.7) \quad \mathcal{L}_{\mathcal{T}}(v; g) = \sum_{K \in \mathcal{T}} \left(\mathbf{div}_{\mathcal{T}} \mathbf{f}(v(\mathbf{z}_K)) \right)^2 |K| + \sum_{E \in \mathcal{E}_-} (v - g)^2(\mathbf{z}_E) |E|,$$

where $|K|$ and $|E|$ are the respective measures of $K \in \mathcal{T}$ and $E \in \mathcal{E}_-$, and $\mathbf{div}_{\mathcal{T}}$ denotes a discrete divergence operator. The discrete divergence operators of the Roe and ENO type were studied in [5]. In the subsequent section, we will introduce new discrete divergence operators tailor to the LSNN method that are accurate approximations to the divergence operator when applying to discontinuous solution.

With the discrete least-squares functional $\mathcal{L}_{\mathcal{T}}(v; g)$, the least-squares neural network (LSNN) method is to find $u_{\mathcal{T}}^N(\mathbf{z}, \boldsymbol{\theta}^*) \in \mathcal{M}_N$ such that

$$(3.8) \quad \mathcal{L}_{\mathcal{T}}(u_{\mathcal{T}}^N(\cdot, \boldsymbol{\theta}^*); g) = \min_{v \in \mathcal{M}_N} \mathcal{L}_{\mathcal{T}}(v(\cdot; \boldsymbol{\theta}); g) = \min_{\boldsymbol{\theta} \in \mathbb{R}^N} \mathcal{L}_{\mathcal{T}}(v(\cdot; \boldsymbol{\theta}); g).$$

LEMMA 3.3. Let u , u^N , and $u_{\mathcal{T}}^N$ be the solutions of problems (2.5), (3.4), and (3.8), respectively. Then we have

$$(3.9) \quad \mathcal{L}(u_{\mathcal{T}}^N; g) \leq \left| (\mathcal{L} - \mathcal{L}_{\mathcal{T}})(u_{\mathcal{T}}^N; g) \right| + \left| (\mathcal{L} - \mathcal{L}_{\mathcal{T}})(u^N; g) \right| + \left| \mathcal{L}(u^N; g) \right|.$$

Proof. By the fact that $\mathcal{L}_{\mathcal{T}}(u_{\mathcal{T}}^N; \mathbf{f}) \leq \mathcal{L}_{\mathcal{T}}(u^N; \mathbf{f})$, we have

$$(3.10) \quad \begin{aligned} \mathcal{L}(u_{\mathcal{T}}^N; g) &= (\mathcal{L} - \mathcal{L}_{\mathcal{T}})(u_{\mathcal{T}}^N; g) + \mathcal{L}_{\mathcal{T}}(u_{\mathcal{T}}^N; g) \leq (\mathcal{L} - \mathcal{L}_{\mathcal{T}})(u_{\mathcal{T}}^N; g) + \mathcal{L}_{\mathcal{T}}(u^N; g) \\ &= (\mathcal{L} - \mathcal{L}_{\mathcal{T}})(u_{\mathcal{T}}^N; g) + (\mathcal{L}_{\mathcal{T}} - \mathcal{L})(u^N; g) + \mathcal{L}(u^N; g), \end{aligned}$$

which, together with the triangle inequality, implies (3.9). \square

This lemma indicates that the minimum of the discrete least-squares functional $\mathcal{L}_{\mathcal{T}}$ over \mathcal{M}_N is bounded by the minimum of the least-squares functional \mathcal{L} over \mathcal{M}_N plus the approximation error of numerical integration and differentiation in \mathcal{M}_N .

In the remainder of this section, we describe the block space-time LSNN method introduced in [5] for dealing with the training difficulty over a relative large computational domain Ω . The method is based on a partition $\{\Omega_{k-1,k}\}_{k=1}^{n_b}$ of the computational domain Ω . To define $\Omega_{k-1,k}$, let $\{\Omega_k\}_{k=1}^{n_b}$ be subdomains of Ω satisfying the following inclusion relation

$$\emptyset = \Omega_0 \subset \Omega_1 \subset \cdots \subset \Omega_{n_b} = \Omega.$$

Then set $\Omega_{k-1,k} = \Omega_k \setminus \Omega_{k-1}$ for $k = 1, \dots, n_b$. Assume that $\Omega_{k-1,k}$ is in the range of influence of

$$\Gamma_{k-1,k} = \partial\Omega_{k-1,k} \cap \partial\Omega_{k-1} \quad \text{and} \quad \Gamma_-^k = \partial\Omega_{k-1,k} \cap \Gamma_-.$$

Denote by $u^k = u|_{\Omega_{k-1,k}}$ the restriction of the solution u of (2.2) on $\Omega_{k-1,k}$, then u^k is the solution of the following problem:

$$(3.11) \quad \begin{cases} \mathbf{div}_{\mathcal{T}} \mathbf{f}(u^k) = 0, & \text{in } \Omega_{k-1,k} \in \mathbb{R}^{d+1}, \\ u^k = u^{k-1}, & \text{on } \Gamma_{k-1,k}, \\ u^k = g, & \text{on } \Gamma_{-}^k. \end{cases}$$

Let

$$\mathcal{L}^k(v; u^{k-1}, g) = \|\mathbf{div} \mathbf{f}(v)\|_{0,\Omega_{k-1,k}}^2 + \|v - u^{k-1}\|_{0,\Gamma_{k-1,k}}^2 + \|v - g\|_{0,\Gamma_{-}^k}^2,$$

and define the corresponding discrete least-squares functional $\mathcal{L}_{\mathcal{T}}^k(v; u^{k-1}, g)$ over the subdomain $\Omega_{k-1,k}$ in a similar fashion as in (3.7). Now, the block space-time LSNN method is to find $u_{\mathcal{T}}^k(\mathbf{z}, \boldsymbol{\theta}_k^*) \in \mathcal{M}_N$ such that

$$(3.12) \quad \mathcal{L}_{\mathcal{T}}^k(u_{\mathcal{T}}^k(\cdot, \boldsymbol{\theta}_k^*); u^{k-1}, g) = \min_{v \in \mathcal{M}_N} \mathcal{L}_{\mathcal{T}}^k(v(\cdot; \boldsymbol{\theta}); u^{k-1}, g) = \min_{\boldsymbol{\theta} \in \mathbb{R}^N} \mathcal{L}_{\mathcal{T}}^k(v(\cdot; \boldsymbol{\theta}); u^{k-1}, g)$$

for $k = 1, \dots, n_b$.

4. Discrete Divergence Operator. As seen in [6, 5], numerical approximation of the differential operator is critical for the success of the LSNN method. Standard numerical or automatic differentiation along coordinate directions generally results in an inaccurate LSNN method, even for linear problems when solutions are discontinuous. This is because the differential form of the HCL is invalid at discontinuous interface. To overcome this difficulty, we used the discrete directional differentiation for linear problems in [6] and the discrete divergence operator of the Roe and ENO type for nonlinear problems in [5].

In this section, we introduce a new discrete divergence operator based on the definition of the divergence operator. Specifically, for each $K \in \mathcal{T}$, by the definition of the divergence operator, we have

$$(4.1) \quad \mathbf{div} \mathbf{f}(u(\mathbf{z}_K)) \approx \text{avg}_K \mathbf{div} \mathbf{f}(u) = \frac{1}{|K|} \int_{\partial K} \mathbf{f}(u) \cdot \mathbf{n} dS,$$

provided that the diameter of K is relatively small, where the average of a function φ over K is defined by

$$\text{avg}_K \varphi = \frac{1}{|K|} \int_K \varphi(\mathbf{z}) d\mathbf{z}.$$

The average of φ with respect to the partition \mathcal{T} is denoted by $\text{avg}_{\mathcal{T}} \varphi$ and defined as a piece-wise constant function through its restriction on each $K \in \mathcal{T}$ by

$$\text{avg}_{\mathcal{T}} \varphi|_K = \text{avg}_K \varphi.$$

Now we may design a discrete divergence operator $\mathbf{div}_{\mathcal{T}}$ acting on the total flux $\mathbf{f}(u)$ by approximating the surface integral on the right-hand side of (4.1).

All existing conservative schemes of various order such as Roe, ENO, WENO, etc. may be viewed as approximations of the surface integral using values of $\mathbf{f}(u)$ at some *mesh points*, where most of them are outside of \bar{K} . These conservative schemes are nonlinear methods because the procedure determining proper mesh points to be used for approximating the average of the spatial flux is a nonlinear process due to possible discontinuity.

Because the LSNN method is a “mesh/point-less” space-time method, all points on $\partial K \in \mathbb{R}^{d+1}$ are at our disposal for approximating the surface integral. Hence, the surface integral can be approximated as accurately as we desire by using only points on ∂K . When u and hence $f_i(u)$ are discontinuous on ∂K , the best linear approximation strategy is to use piece-wise constant/linear

functions on a sufficiently fine partition of each face of ∂K , instead of higher order polynomials on each face. This suggests that a composite lower-order numerical integration such as the composite mid-point/trapezoidal quadrature would provide accurate approximation to the surface integral in (4.1), and hence the resulting discrete divergence operator would be accurate approximation to the divergence operator, even if the solution is discontinuous.

4.1. One Dimension. For clarity of presentation, the discrete divergence operator described above will be first introduced in this section in one dimension. To this end, to approximate single integral $I(\varphi) = \int_c^d \varphi(s) ds$, we will use the composite mid-point/trapezoidal rule:

$$(4.2) \quad Q(\varphi(s); c, d, p) = \begin{cases} \frac{d-c}{p} \sum_{i=0}^{p-1} \varphi(s_{i+1/2}), & \text{midpoint,} \\ \frac{d-c}{2p} \left(\varphi(c) + \varphi(d) + 2 \sum_{i=1}^{p-1} \varphi(s_i) \right), & \text{trapezoidal,} \end{cases}$$

where $\{s_i\}_{i=0}^p$ uniformly partitions the interval $[c, d]$ into p sub-intervals.

Let $\Omega = (a, b) \times (0, T)$. For simplicity, assume that the integration partition \mathcal{T} introduced in Section 3 is a uniform partition of the domain Ω ; i.e.,

$$\mathcal{T} = \{K = K_{ij} : i = 0, 1, \dots, m-1; j = 0, 1, \dots, n-1\} \text{ with } K_{ij} = (x_i, x_{i+1}) \times (t_j, t_{j+1}),$$

where $x_i = a + ih$ and $t_j = j\tau$ with $h = (b-a)/m$ and $\delta = T/n$. Denote the centroid of $K \in \mathcal{T}$ by

$$\mathbf{z}_K = \mathbf{z}_{ij} = (x_i + h/2, t_j + \delta/2).$$

Denote by $\sigma = f(u)$ the spatial flux, then the total flux is the two-dimensional vector field $\mathbf{f}(u) = (\sigma, u)$. Denote the first-order finite difference quotients by

$$\sigma(x_i, x_{i+1}; t) = \frac{\sigma(x_{i+1}, t) - \sigma(x_i, t)}{x_{i+1} - x_i} \quad \text{and} \quad u(x; t_j, t_{j+1}) = \frac{u(x, t_{j+1}) - u(x, t_j)}{t_{j+1} - t_j}.$$

Then the surface integral in (4.1) becomes

$$(4.3) \quad \frac{1}{|K_{ij}|} \int_{\partial K_{ij}} \mathbf{f}(u) \cdot \mathbf{n} dS = \delta^{-1} \int_{t_j}^{t_{j+1}} \sigma(x_i, x_{i+1}; t) dt + h^{-1} \int_{x_i}^{x_{i+1}} u(x; t_j, t_{j+1}) dx.$$

Approximating single integrals by the composite mid-point/trapezoidal rule, we obtain the following discrete divergence operator

$$(4.4) \quad \mathbf{div}_\tau \mathbf{f}(u(\mathbf{z}_{ij})) = \delta^{-1} Q(\sigma(x_i, x_{i+1}; t); t_j, t_{j+1}, \hat{n}) + h^{-1} Q(u(x; t_j, t_{j+1}); x_i, x_{i+1}, \hat{m}).$$

REMARK 4.1. Denote by $u_{i,j}$ as approximation to $u(x_i, t_j)$. (4.4) with $\hat{m} = \hat{n} = 1$ using the trapezoidal rule leads to the following implicit conservative scheme for the one-dimensional scalar nonlinear HCL:

$$(4.5) \quad \frac{u_{i+1,j+1} + u_{i,j+1}}{\delta} + \frac{f(u_{i+1,j+1}) - f(u_{i,j+1})}{h} = \frac{u_{i+1,j} + u_{i,j}}{\delta} - \frac{f(u_{i+1,j}) - f(u_{i,j})}{h}$$

for $i = 0, 1, \dots, m-1$ and $j = 0, 1, \dots, n-1$.

Below, we state error estimates of the discrete divergence operator defined in (4.4) and postpone their proof to Appendix.

LEMMA 4.2. *For any $K_{ij} \in \mathcal{T}$, assume that u is a C^2 function on every edge of the rectangle ∂K_{ij} . Then there exists a constant $C > 0$ such that*

$$(4.6) \quad \begin{aligned} & \|\mathbf{div}_\tau \mathbf{f}(u) - \text{avg}_\tau \mathbf{div} \mathbf{f}(u)\|_{L^p(K_{ij})} \\ & \leq C \left(\frac{h^{1/p} \delta^2}{\hat{n}^2} \|\sigma_{tt}(x_{i+1}, x_i; \cdot)\|_{L^p(t_j, t_{j+1})} + \frac{h^2 \delta^{1/p}}{\hat{m}^2} \|u_{xx}(\cdot; t_{j+1}, t_j)\|_{L^p(x_i, x_{i+1})} \right). \end{aligned}$$

This lemma indicates that $\hat{m} = 1$ and $\hat{n} = 1$ are sufficient if the solution is smooth on ∂K_{ij} . In this case, we may use higher order numerical integration, e.g., the Gauss quadrature, to approximate the surface integral in (4.3) for constructing a higher order discrete divergence operator.

When u is discontinuous on ∂K_{ij} , error estimate on the discrete divergence operator becomes more involved. To this end, first we consider the case that the discontinuous interface Γ_{ij} (a straight line) intersects two horizontal boundary edges of K_{ij} . Denote by $u_{ij} = u|_{K_{ij}}$ the restriction of u in K_{ij} and by $\llbracket u_{ij} \rrbracket_{t_l}$ the jump of u_{ij} on the horizontal boundary edge $t = t_l$ of K_{ij} , where $l = j$ and $l = j + 1$.

LEMMA 4.3. *Assume that u is a C^2 function of t and a piece-wise C^2 function of x on two vertical and two horizontal edges of K_{ij} , respectively. Moreover, u has only one discontinuous point on each horizontal edge. Then there exists a constant $C > 0$ such that*

$$(4.7) \quad \|\mathbf{div}_\tau \mathbf{f}(u) - \text{avg}_\tau \mathbf{div} \mathbf{f}(u)\|_{L^p(K_{ij})} \leq C \left(\frac{h^{1/p} \delta^2}{\hat{n}^2} + \frac{h^2 \delta^{1/p}}{\hat{m}^2} + \frac{h \delta^{1/p}}{\hat{m}^{1+1/q}} \right) + \frac{(h\delta)^{1/p}}{\hat{m}} \sum_{l=j}^{j+1} \llbracket u_{ij} \rrbracket_{t_l}.$$

REMARK 4.4. Lemma 4.3 implies that the choice of the number of sub-intervals of (x_i, x_{i+1}) on the composite numerical integration depends on the size of the jump of the solution and that large \hat{m} would guarantee accuracy of the discrete divergence operator when u is discontinuous on ∂K_{ij} .

REMARK 4.5. *Error bounds similar to (4.7) hold for the other cases: Γ_{ij} intercepts (i) two vertical edges or (ii) one horizontal and one vertical edges of K_{ij} . Specifically, we have*

$$\|\mathbf{div}_\tau \mathbf{f}(u) - \text{avg}_\tau \mathbf{div} \mathbf{f}(u)\|_{L^p(K_{ij})} \leq C \left(\frac{h^{1/p} \delta^2}{\hat{n}^2} + \frac{h^2 \delta^{1/p}}{\hat{m}^2} + \frac{h^{1/p} \delta}{\hat{n}^{1+1/q}} \right) + \frac{(h\delta)^{1/p}}{\hat{n}} \sum_{l=i}^{i+1} \llbracket \sigma_{ij} \rrbracket_{x_l}$$

for the case (i) and

$$\|\mathbf{div}_\tau \mathbf{f}(u) - \text{avg}_\tau \mathbf{div} \mathbf{f}(u)\|_{L^p(K_{ij})} \leq C \left(\frac{h^{1/p} \delta^2}{\hat{n}^2} + \frac{h^2 \delta^{1/p}}{\hat{m}^2} + \frac{h \delta^{1/p}}{\hat{m}^{1+1/q}} + \frac{h^{1/p} \delta}{\hat{n}^{1+1/q}} \right) + E_{ij}$$

for the case (ii), where $E_{ij} = (h\delta)^{1/p} \left(\frac{1}{\hat{m}} \llbracket u_{ij} \rrbracket_{t_l} + \frac{1}{\hat{n}} \llbracket \sigma_{ij} \rrbracket_{x_l} \right)$ with $x_l = x_i$ or x_{i+1} and $t_l = t_j$ or t_{j+1} .

4.2. Two Dimensions. This section describes the discrete divergence operator in two dimensions. As in one dimension, the discrete divergence operator is defined as an approximation to the average of the divergence operator through the composite mid-point/trapezoidal quadrature to approximate the surface integral (4.1). Extension to three dimensions is straightforward.

To this end, we first describe the composite mid-point/trapezoidal numerical integration for approximating a double integral over a rectangle region $T = (c_1, d_1) \times (c_2, d_2)$

$$\begin{aligned} I(\varphi) &= \int_T \varphi(s_1, s_2) ds_1 ds_2 \\ &\approx Q(\varphi(s_1, s_2); c_1, d_1, p_1; c_2, d_2, p_2) \equiv Q\left(Q(\varphi(s_1, \cdot); c_1, d_1, p_1)(s_2); c_2, d_2, p_2\right), \end{aligned}$$

where $Q(\varphi(s_1, \cdot); c_1, d_1, p_1)$ is the composite quadrature defined in (4.2).

For simplicity, let $\Omega = \tilde{\Omega} \times I = (a_1, b_1) \times (a_2, b_2) \times (0, T)$, and assume that the integration partition \mathcal{T} introduced in Section 3 is a uniform partition of the domain Ω ; i.e.,

$$\mathcal{T} = \{K = K_{ijk} : i = 0, 1, \dots, m_1 - 1; j = 0, 1, \dots, m_2 - 1; k = 0, 1, \dots, n - 1\}$$

with $K_{ijk} = (x_i, x_{i+1}) \times (y_j, y_{j+1}) \times (t_k, t_{k+1})$, where

$$x_i = a_1 + ih_1, \quad y_j = a_2 + jh_2, \quad \text{and} \quad t_k = k\delta,$$

and $h_l = (b_l - a_l)/m_l$ for $l = 1, 2$ and $\delta = T/n$ are the respective spatial and temporal sizes of the integration mesh. Denote the mid-point of K_{ijk} by

$$\mathbf{z}_{ijk} = \left(x_i + \frac{h_1}{2}, y_j + \frac{h_2}{2}, t_k + \frac{\delta}{2}\right).$$

Let $\boldsymbol{\sigma} = (\sigma_1, \sigma_2) = (f_1(u), f_2(u))$, then the space-time flux is the three-dimensional vector field: $\mathbf{f}(u) = (\boldsymbol{\sigma}, u) = (\sigma_1, \sigma_2, u)$. Denote the the first-order finite difference quotients by

$$\sigma_1(y, t; x_i, x_{i+1}) = \frac{\sigma_1(x_{i+1}, y, t) - \sigma_1(x_i, y, t)}{x_{i+1} - x_i}, \quad \sigma_2(x, t; y_j, y_{j+1}) = \frac{\sigma_2(x, y_{j+1}, t) - \sigma_2(x, y_j, t)}{y_{j+1} - y_j},$$

$$\text{and } u(x, y; t_k, t_{k+1}) = \frac{u(x, y, t_{k+1}) - u(x, y, t_k)}{t_{k+1} - t_k}.$$

Denote three faces of ∂K_{ijk} by

$$K_{ij}^{xy} = (x_i, x_{i+1}) \times (y_j, y_{j+1}), \quad K_{ik}^{xt} = (x_i, x_{i+1}) \times (t_k, t_{k+1}), \quad \text{and} \quad K_{jk}^{yt} = (y_j, y_{j+1}) \times (t_k, t_{k+1}).$$

Then the surface integral in (4.1) becomes

$$(4.8) \quad \frac{1}{|K_{ijk}|} \int_{\partial K_{ijk}} \mathbf{f}(u) \cdot \mathbf{n} dS = (h_2\delta)^{-1} \int_{K_{jk}^{yt}} \sigma_1(y, t; x_{i+1}, x_i) dydt \\ + (h_1\delta)^{-1} \int_{K_{ik}^{xt}} \sigma_2(x, t; y_{j+1}, y_j) dxdt + (h_1h_2)^{-1} \int_{K_{ij}^{xy}} u(x, y; t_{k+1}, t_k) dx dy.$$

Approximating double integrals by the composite midpoint/trapezoidal rule, we obtain the following discrete divergence operator

$$(4.9) \quad \text{div}_T \mathbf{f}(u(\mathbf{z}_{ijk})) = (h_2\delta)^{-1} Q(\sigma_1(y, t; x_{i+1}, x_i); y_j, y_{j+1}, \hat{m}_2; t_k, t_{k+1}, \hat{n}) \\ + (h_1\delta)^{-1} Q(\sigma_2(x, t; y_{j+1}, y_j); x_i, x_{i+1}, \hat{m}_1; t_k, t_{k+1}, \hat{n}) \\ + (h_1h_2)^{-1} Q(u(x, y; t_{k+1}, t_k); x_i, x_{i+1}, \hat{m}_1; y_j, y_{j+1}, \hat{m}_2).$$

4.3. Integration mesh size. The discrete divergence operator defined in (4.4) and (4.9) for the respective one- and two- dimension is based on the composite midpoint/trapezoidal rule. As shown in Lemmas 4.2 and 4.3 and Remark 4.5, the discrete divergence operator can be as accurate as desired for the discontinuous solution provided that the size of integration mesh is sufficiently small.

To reduce computational cost, note that the discontinuous interfaces of the solution u lie on d -dimensional hyper-planes. Hence, they only intersect with a small portion of control volumes in \mathcal{T} . This observation suggests that sufficiently fine meshes are only needed for control volumes

at where the solution is possibly discontinuous. To realize this idea, we divide the set of control volumes into two subsets:

$$\mathcal{T} = \mathcal{T}_c \cup \mathcal{T}_d,$$

where the solution u is continuous in each control volume of \mathcal{K}_c^l and possibly discontinuous at some control volumes of \mathcal{T}_d ; i.e.,

$$\mathcal{T}_c = \{K \in \mathcal{T} : u \in C(K)\} \quad \text{and} \quad \mathcal{T}_d = \mathcal{T} \setminus \mathcal{T}_c.$$

Next, we describe how to determine the set of control volumes \mathcal{T}_d in one dimension by the range of influence. It is well-known that characteristic curves are straight lines before their interception and are given by

$$(4.10) \quad x = x(T_l) + (t - T_l) f'(u(x(T_l), T_l)).$$

For $i = 0, 1, \dots, m$, let

$$\hat{x}_i = x_i + (T_{l+1} - T_l) f'(u_N^l(x_i, T_l)),$$

where $u_N^l(x_i, T_l)$ is the neural network approximation from the previous time block

$$\Omega \times I_{l-1} = (a, b) \times (T_{l-1}, T_l).$$

Clearly, the solution u is discontinuous in a control volume $V_i \times I_i^k$ if either (1) $u(x, T_l)$ is discontinuous at the interval V_i or (2) there are two characteristic lines intercepting in $V_i \times I_i^k$. In the first case, $V_i \times I_i^k$ is in \mathcal{K}_d^l if $u_N^l(x, T_l)$ has a sharp change in the interval V_i ; moreover, either $V_{i-1} \times I_i^k \in \mathcal{K}_d^l$ if $\hat{x}_i < x_i$ or $V_{i+1} \times I_i^k \in \mathcal{K}_d^l$ if $\hat{x}_{i+1} > x_{i+1}$. In the second case, assume that $\hat{x}_i > \hat{x}_{i+1}$, then $V_i \times I_i^k \in \mathcal{K}_d^l$ if $\hat{x}_i < x_{i+1}$.

5. Numerical Experiments. This section presents numerical results of the block space-time LSNN method for one and two dimensional problems. Let $\Omega = \tilde{\Omega} \times (0, T)$. The k^{th} space-time block is defined as

$$\Omega_{k-1,k} = \Omega_k \setminus \Omega_{k-1} = \tilde{\Omega} \times \left(\frac{(k-1)T}{n_b}, \frac{kT}{n_b} \right) \quad \text{for } k = 1, \dots, n_b,$$

where $\Omega_k = \tilde{\Omega} \times (0, kT/n_b)$. For efficient training, the least-squares functional is modified as follows:

$$(5.1) \quad \mathcal{L}^k(v; u^{k-1}, g) = \|\mathbf{div} \mathbf{f}(v)\|_{0, \Omega_{k-1,k}}^2 + \alpha (\|v - u^{k-1}\|_{0, \Gamma_{k-1,k}}^2 + \|v - g\|_{0, \Gamma_k^-}^2),$$

where α is a weight to be chosen empirically.

Unless otherwise stated, the integration mesh \mathcal{T}_k is a uniform partition of $\Omega_{k-1,k}$ with $h = \delta = 0.01$, and the discrete divergence operator defined in (4.4) is based on the composite trapezoidal rule with $\hat{n} = \hat{n} = 2$. Three-layer or four-layer neural network are employed for all test problems and are denoted by $d_i n - n_1 - n_2 (-n_3) - 1$ with n_1, n_2 and n_3 neurons in the respective first, second and third (for a four-layer NN) layers. The same network structure is used for all time blocks.

The network is trained by using the ADAM [23] (a variant of the method of gradient descent) with either a fixed or an adaptive learning rate to iteratively solve the minimization problem in (3.12). Parameters of the first block is initialized by an approach introduced in [26], and those for the current block is initialized by using the NN approximation of the previous block (see Remark 4.1 of [5]).

The solution of the problem in (3.11) and its corresponding NN approximation are denoted by u^k and $u_{\mathcal{T}}^k$, respectively. Their traces are depicted on a plane of given time and exhibit capability of the numerical approximation in capturing shock/rarefaction.

TABLE 5.1
Relative L^2 errors of Riemann problem (shock) for Burgers' equation

Network structure	Block	$\frac{\ u^k - u^k_{\mathcal{T}}\ _0}{\ u^k\ _0}$
2-10-10-1	$\Omega_{0,1}$	0.048774
	$\Omega_{1,2}$	0.046521
	$\Omega_{2,3}$	0.044616

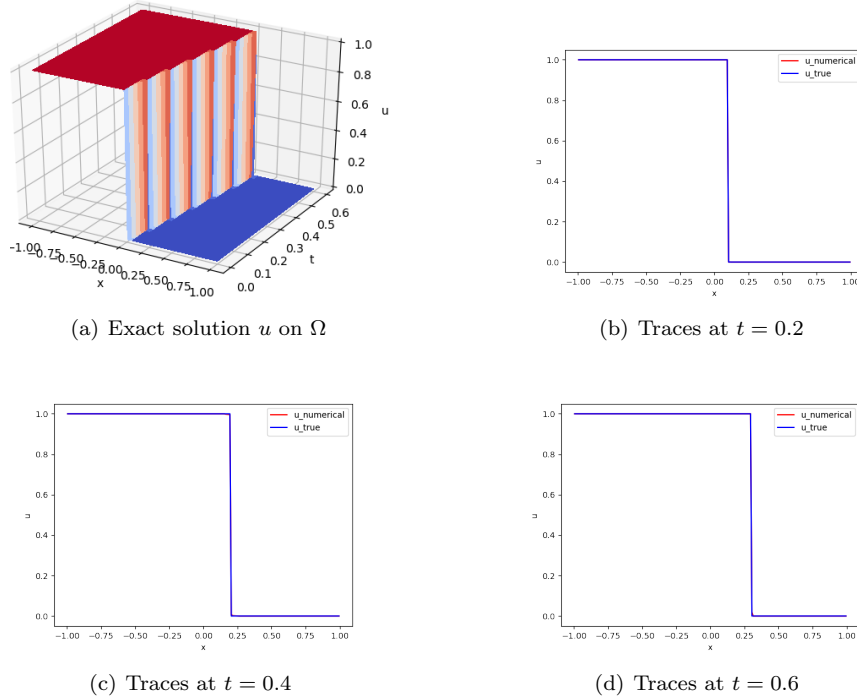


FIG. 5.1. Approximation results of Riemann problem (shock) for Burgers' equation

5.1. Inviscid Burgers' equation. This section reports numerical results of the block space-time LSNN method for the one dimensional inviscid Burgers equation, where the spatial flux is $\tilde{f}(u) = f(u) = \frac{1}{2}u^2$.

The first two test problems are the Riemann problem with the initial condition: $u_0(x) = u(x, 0) = u_L$ if $x \leq 0$ or u_R if $x \geq 0$.

Shock formation. When $u_L = 1 > 0 = u_R$, a shock is formed immediately with the shock speed $s = (u_L + u_R)/2$. The first test problem is defined on a computational domain $\Omega = (-1, 1) \times (0, 0.6)$ with inflow boundary

$$\Gamma_- = \Gamma_-^L \cup \Gamma_-^R \equiv \{(-1, t) : t \in [0, 0.6]\} \cup \{(1, t) : t \in [0, 0.6]\}$$

and boundary conditions: $g = u_L = 1$ on Γ_-^L and $g = u_R = 0$ on Γ_-^R . With $n_b = 3$ blocks, weight $\alpha = 20$, a fixed learning rate 0.003, and 30000 iterations for each block, the relative errors in the L^2 norm are reported in Table 5.1. Traces of the exact solution and numerical approximation on the planes $t = kT/n_b$ for $k = 1, 2, 3$ are depicted in Fig. 5.1(b)-(d), which clearly indicate that the LSNN method is capable of capturing the shock formation and its speed. Moreover, it approximates the solution well without oscillations.

TABLE 5.2
Relative L^2 errors of Riemann problem (rarefaction) for Burgers' equation

Network structure	Block	$\frac{\ u^k - u^k_\tau\ _0}{\ u^k\ _0}$
2-10-10-1	$\Omega_{0,1}$	0.013387
	$\Omega_{1,2}$	0.010079

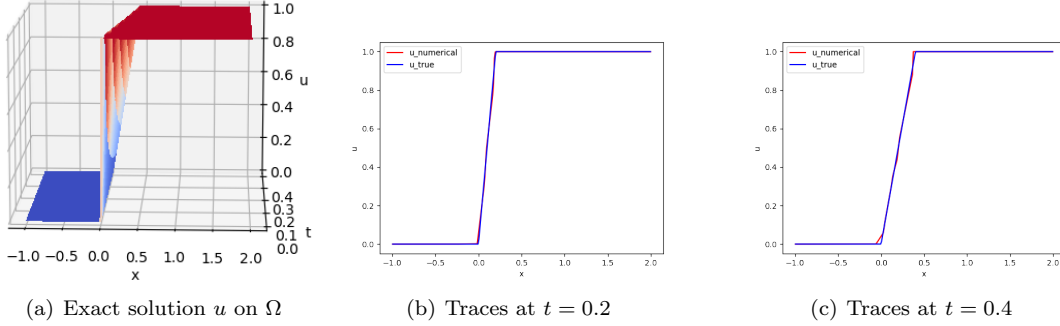


FIG. 5.2. Approximation results of Riemann problem (rarefaction) for Burgers' equation

Rarefaction waves. When $u_L = 0 < 1 = u_R$, the range of influence of all points in \mathbb{R} is a proper subset of $\mathbb{R} \times [0, \infty)$. Hence, the weak solution of the scalar hyperbolic conservation law is not unique. The second test problem is defined on a computational domain $\Omega = (-1, 2) \times (0, 0.4)$ with inflow boundary condition $g = 0$ on $\Gamma_- = \{(-1, t) : t \in [0, 0.4]\}$. As shown in Section 5.1.2 of [5], the LSNN method using Roe's scheme has a limitation to resolve the rarefaction. Numerical results of the LSNN method using the discrete divergence operator ($n_b = 2$, $\alpha = 10$, a fixed learning rate 0.003, and 40000 iterations) are reported in Table 5.2. Traces of the exact solution and numerical approximation on the planes $t = 0.2$ and $t = 0.4$ are depicted in Fig. 5.2. This test problem shows that the LSNN method using the \mathbf{div}_τ is able to compute the physically relevant vanishing viscosity solution (see, e.g., [24, 33]) without special treatment. This is possibly due to the fact that the LSNN approximation is continuous.

Sinusoidal initial condition. The third test problem has smooth initial condition $u_0(x) = 0.5 + \sin(\pi x)$ and is defined on the computational domain $\Omega = (0, 2) \times (0, 0.8)$ with inflow boundary

$$\Gamma_- = \Gamma_-^L \cup \Gamma_-^R \equiv \{(0, t) : t \in [0, 0.8]\} \cup \{(2, t) : t \in [0, 0.8]\}.$$

The shock of the problem appears at $t = 1/\pi \approx 0.318$. This is the same test problem as in Section 5.2 of [5] (see also [22, 34]). The goal of this experiment is to compare numerical performances of the LSNN methods using the \mathbf{div}_τ introduced in this paper and the ENO scheme in [5].

Since the solution of this problem is implicitly given, to accurately measure the quality of NN approximations, a benchmark reference solution \hat{u} is generated using the traditional mesh-based method. In particular, the third-order accurate WENO scheme [30] and the fourth-order Runge-Kutta method are employed for the respective spatial and temporal discretizations with a fine mesh ($\Delta x = 0.001$ and $\Delta t = 0.0002$) on the computational domain Ω .

The LSNN using \mathbf{div}_τ is implemented with the same set of hyper parameters as in Section 5.2 of [5], i.e., training weight $\alpha = 5$ and an adaptive learning rate which starts with 0.005 and reduces by half for every 25000 iterations. Setting $n_b = 16$ and on each time block, the total number of iterations is set as 50000 and the size of the NN model is 2-30-30-1. Although we observe some error accumulation when the block evolves for both the LSNN methods, the one using \mathbf{div}_τ performs better than that using ENO (see Table 5.3 for the relative L^2 norm error and Fig. 5.3(a)-(h) for

graphs near the left side of the interface).

TABLE 5.3
Relative L^2 errors of Burgers' equation with a sinusoidal initial condition

Network structure	Block	LSNN using \mathbf{div}_τ	LSNN using ENO [5]
		$\frac{\ u^k - u_\tau^k\ _0}{\ u^k\ _0}$	$\frac{\ u^k - u_\tau^k\ _0}{\ u^k\ _0}$
2-30-30-1	$\Omega_{0,1}$	0.010641	0.010461
	$\Omega_{1,2}$	0.011385	0.012517
	$\Omega_{2,3}$	0.012541	0.019772
	$\Omega_{3,4}$	0.014351	0.022574
	$\Omega_{4,5}$	0.016446	0.029011
	$\Omega_{5,6}$	0.018634	0.038852
	$\Omega_{6,7}$	0.031103	0.075888
	$\Omega_{7,8}$	0.053114	0.078581
	$\Omega_{8,9}$	0.053562	–
	$\Omega_{9,10}$	0.064933	–
	$\Omega_{10,11}$	0.061354	–
	$\Omega_{11,12}$	0.077982	–
	$\Omega_{12,13}$	0.061145	–
	$\Omega_{13,14}$	0.070554	–
	$\Omega_{14,15}$	0.068539	–
	$\Omega_{15,16}$	0.065816	–

TABLE 5.4
Relative L^2 errors of the problem with $f(u) = \frac{1}{4}u^4$ using the composite trapezoidal rule (4.2)

Time block	Number of sub-intervals		
	$\hat{m} = \hat{n} = 2$	$\hat{m} = \hat{n} = 4$	$\hat{m} = \hat{n} = 6$
$\Omega_{0,1}$	0.067712	0.010446	0.004543
$\Omega_{1,2}$	0.108611	0.008275	0.009613

TABLE 5.5
Relative L^2 errors of the problem with $f(u) = \frac{1}{4}u^4$ using the composite mid-point rule (4.2)

Time block	Number of sub-intervals		
	$\hat{m} = \hat{n} = 2$	$\hat{m} = \hat{n} = 4$	$\hat{m} = \hat{n} = 6$
$\Omega_{0,1}$	0.096238	0.007917	0.003381
$\Omega_{1,2}$	0.159651	0.007169	0.005028

5.2. Riemann problem with $f(u) = \frac{1}{4}u^4$. The goals of this set of numerical experiments are twofold. First, we compare the performance of the LSNN method using the composite trapezoidal/mid-point rule in (4.2). Second, we investigate the impact of the number of sub-intervals of the composite quadrature rule on the accuracy of the LSNN method.

The test problem is the Riemann problem with a convex flux $\mathbf{f}(u) = (f(u), u) = (\frac{1}{4}u^4, u)$ and the initial condition $u_L = 1 > 0 = u_R$. The computational domain is chosen to be $\Omega = (-1, 1) \times (0, 0.4)$. Relative L^2 errors of the LSNN method using the \mathbf{div}_τ (2-10-10-1 NN model, $n_b = 2$, $\alpha = 20$, a fixed learning rate 0.003 for the first 30000 iterations and 0.001 for the remaining)

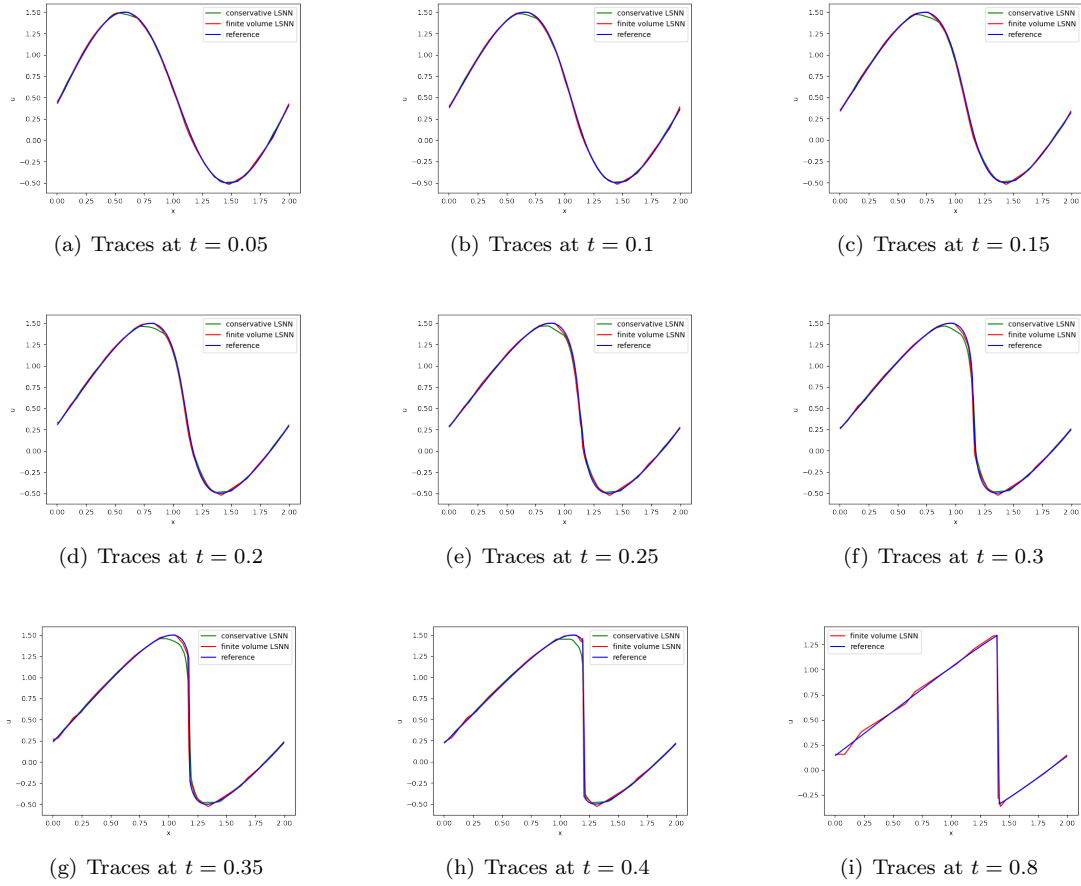


FIG. 5.3. Approximation results of Burgers' equation with a sinusoidal initial condition

are reported in Tables 5.4 and 5.5; and traces of the exact and numerical solutions are depicted in Fig. 5.4.

Clearly, Tables 5.4 and 5.5 indicate that the accuracy of the LSNN method depends on the number of sub-intervals (\hat{m} and \hat{n}) for the composite quadrature rule; i.e., the larger \hat{m} and \hat{n} are, the more accurate the LSNN method is. Moreover, the accuracy using the composite trapezoidal and mid-point rules in the LSNN method is comparable.

TABLE 5.6
Relative L^2 errors of Riemann problem with a non-convex flux $f(u) = \frac{1}{3}u^3$

Network structure	Block	$\frac{\ u^k - u_{\mathcal{T}}^k\ _0}{\ u^k\ _0}$
2-64-64-64-1	$\Omega_{0,1}$	0.03277
	$\Omega_{1,2}$	0.03370
	$\Omega_{2,3}$	0.03450
	$\Omega_{3,4}$	0.03578

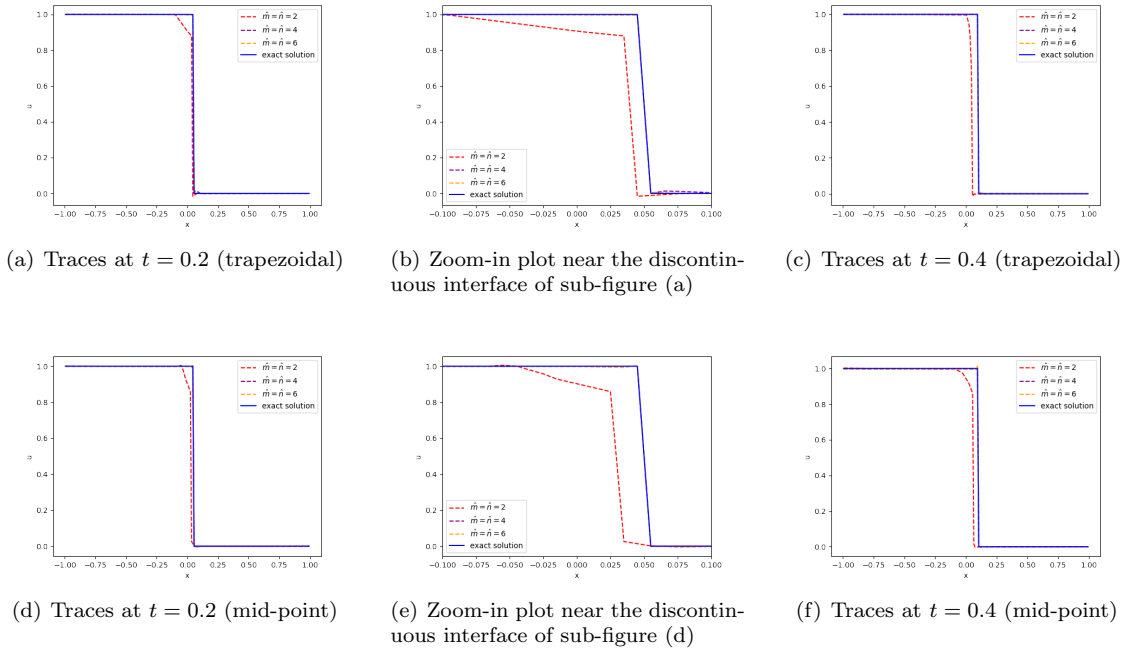


FIG. 5.4. Numerical results of the problem with $f(u) = \frac{1}{4}u^4$ using the composite trapezoidal and mid-point rules

5.3. Riemann problem with non-convex fluxes. The test problem for a non-convex flux is a modification of the test problem in Section 5.2 by replacing the flux with $f(u) = \frac{1}{3}u^3$ and the initial condition with $u_L = 1 > -1 = u_R$. The Riemann solution consists partly of a rarefaction wave together with a shock wave which brings a new level of challenge with a compound wave. The exact solution is obtained through Osher's formulation [27] which has a shock speed $s=0.25$ and a shock jump from 1 to -0.5 when $t > 0$.

The block space-time LSNN method using the \mathbf{div}_τ with $\hat{m} = \hat{n} = 4$ is utilized for this problem. Four time blocks are computed on the temporal domain $(0, 0.4)$ and a relative larger network structure (2-64-64-64-1) is tested with a smaller integration mesh size $h = \delta = 0.005$ to compute the compound wave more precisely. We tune the hyper parameter $\alpha = 200$, and all time blocks are computed with a total of 60000 iterations (learning rate starts with 1e-3 and decay to 20% every 20000 iterations). Due to the random initial guess for the second hidden layer parameters, the experiment is replicated several times. Similar results are obtained as the best result reported in Table 5.6 and Fig. 5.5 (a)-(e). These experiments demonstrate that the LSNN method can capture the compound wave for non-convex flux problems as well.

5.4. Two-dimensional problem. Consider a two-dimensional inviscid Burgers equation, where the spatial flux vector field is $\tilde{\mathbf{f}}(u) = \frac{1}{2}(u^2, u^2)$. Given a piece-wise constant initial data

$$(5.2) \quad u_0(x, y) = \begin{cases} -0.2, & \text{if } x < 0.5 \text{ and } y > 0.5, \\ -1.0, & \text{if } x > 0.5 \text{ and } y > 0.5, \\ 0.5, & \text{if } x < 0.5 \text{ and } y < 0.5, \\ 0.8, & \text{if } x > 0.5 \text{ and } y < 0.5, \end{cases}$$

this problem has an exact solution given in [16].

The test problem is set on computational domain $\Omega = (0, 1)^2 \times (0, 0.5)$ with inflow boundary

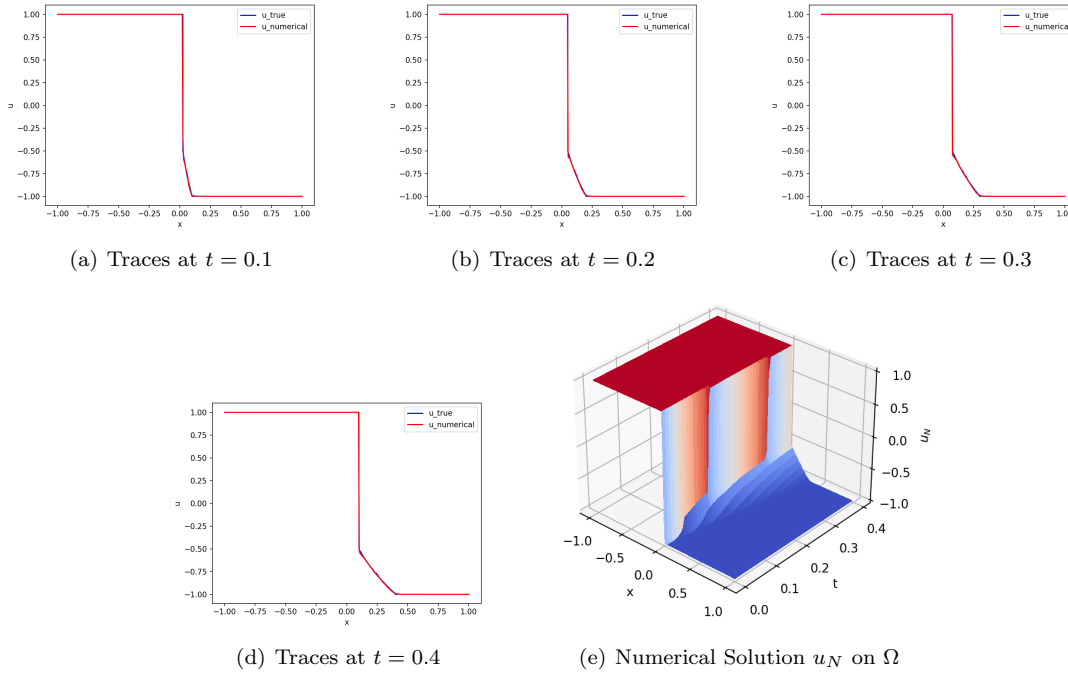


FIG. 5.5. Numerical results of Riemann problem with a non-convex flux $f(u) = \frac{1}{3}u^3$

conditions prescribed by using the exact solution. Our numerical result using a 4-layer LSNN (3-48-48-48-1) with $3D \mathbf{div}_{\mathcal{T}} (\hat{m} = \hat{n} = \hat{k} = 2)$ are reported in Table 5.7. The corresponding hyper parameters setting is as follows: $n_b = 5$, $\alpha = 20$, the first time block is trained with 30000 iteration where the first 10000 iterations are using learning rate 0.003 and the rest iterations are trained using learning rate of 0.001; all remaining time blocks are trained with 20000 iterations using fixed learning rate of 0.001. Fig. 5.6 presents the graphical results at time $t = 0.1, 0.3$, and 0.5 . This experiment shows that the proposed LSNN method can be extended to two dimensional problems and can capture the shock and rarefaction waves in two dimensions.

TABLE 5.7
Relative L^2 errors of Riemann problem (shock) for 2D Burgers' equation

Network structure	Block	$\frac{\ u^k - u_{\mathcal{T}}^k\ _0}{\ u^k\ _0}$
3-48-48-48-1	$\Omega_{0,1}$	0.093679
	$\Omega_{1,2}$	0.121375
	$\Omega_{2,3}$	0.163755
	$\Omega_{3,4}$	0.190460
	$\Omega_{4,5}$	0.213013

6. Discussion and Conclusion. The ReLU neural network provides a new class of approximating functions that is particularly suitable for problems having discontinuous solution with unknown interface location [6]. However, NN-based methods introduced in [1, 14, 28] are not applicable to problems with shock. Such a failure is due to improper approximation to differential operator of the underlying problem.

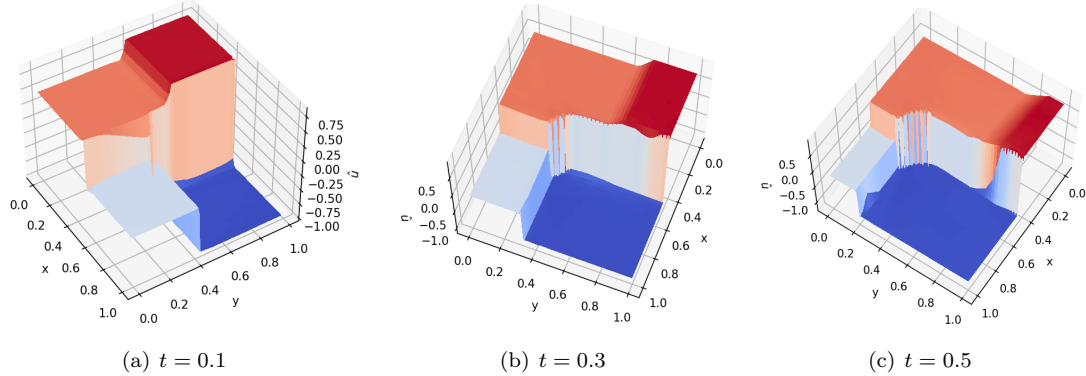


FIG. 5.6. Numerical results of 2D Burgers' equation.

By employing discrete differential operator of conservative methods [24] using Roe or ENO flux, in [5] we introduced the first NN-based method that is capable of capturing shock without oscillation or smearing for scalar nonlinear hyperbolic conservation laws with convex spatial fluxes $f(u) = \frac{1}{2}u^2$ and $\frac{1}{4}u^4$. As pointed out in [5] that the method is inaccurate for complicated initial condition and has limitations for problems with rarefaction waves and with non-convex spatial fluxes.

To overcome deficiencies of our method in [5], this paper introduces a new discrete divergence operator \mathbf{div}_τ . Both the \mathbf{div}_τ operator and the discrete differential operator used in [5] are based on surface integrals over boundary of control volumes. But they differ in how to approximate those surface integrals: the former uses only boundary points of the control volume while the latter uses *mesh-points* outside of the control volume (see Section 4 for details). Moreover, the former is a linear operator while the latter is nonlinear.

Numerical results for several test problems show that the LSNN method using the \mathbf{div}_τ do overcome drawbacks of the LSNN method with ENO flux in [5]. Moreover, for the one dimensional test problems with fluxes $f(u) = \frac{1}{4}u^4$ and $\frac{1}{3}u^3$, accuracy of the method may be improved greatly by using enough number of sub-intervals in the composite trapezoidal/mid-point quadrature.

Even though the number of degrees of freedom for the LSNN method is several order of magnitude less than those of traditional mesh-based numerical methods, training NN is computationally intensive and complicated. For a network with more than one hidden layer, random initialization of the parameters in layers beyond the first hidden layer would cause some uncertainty in training NN (iteratively solving the resulting non-convex optimization) as observed in Section 5.2. This issue plus designation of a proper architecture of NN would be addressed in a forthcoming paper using the adaptive network enhancement (ANE) method developed in [26, 25, 7].

REFERENCES

- [1] Y. Bar-Sinai, S. Hoyer, J. Hickey, and M. P. Brenner. Learning data-driven discretizations for partial differential equations. *Proceedings of the National Academy of Science of USA*, 116 (31):15344–15349, 2019.
- [2] P. Bochev and J. Choi. Improved least-squares error estimates for scalar hyperbolic problems. *Comput. Methods Appl. Math.*, 1(2):115–124, 2001.
- [3] F. Brezzi, L. D. Marini, and E. Süli. Discontinuous Galerkin methods for first-order hyperbolic problems. *Math. Models Methods Appl. Sci.*, 14(12):1893–1903, 2004.
- [4] E. Burman. A posteriori error estimation for interior penalty finite element approximations of the advection-reaction equation. *SIAM J. Numer. Anal.*, 47(5):3584–3607, 2009.
- [5] Z. Cai, J. Chen, and M. Liu. Least-squares ReLU neural network (LSNN) method for scalar nonlinear hyperbolic conservation law. *Appl. Numer. Math.*, 174:163–176, 2022.
- [6] Z. Cai, J. Chen, and M. Liu. Least-squares ReLU neural network (LSNN) method for linear advection-reaction

- equation. *J. Comput. Phys.*, 443 (2021) 110514.
- [7] Z. Cai, J. Chen, and M. Liu. Self-adaptive deep neural network: Numerical approximation to functions and PDEs. *J. Comput. Phys.*, 455 (2022) 111021.
 - [8] Z. Cai, J. Chen, M. Liu, and X. Liu. Deep least-squares methods: An unsupervised learning-based numerical method for solving elliptic PDEs. *J. Comput. Phys.*, 420 (2020) 109707.
 - [9] B. Cockburn and C.-W. Shu. TVB Runge-Kutta local projection discontinuous galerkin finite element method for conservation laws. *Math. Comp.*, 52:411–435, 1989.
 - [10] W. Dahmen, C. Huang, C. Schwab, and G. Welper. Adaptive petrov–galerkin methods for first order transport equations. *SIAM J. Numer. Anal.*, 50(5):2420–2445, 2012.
 - [11] H. De Sterck, T. A. Manteuffel, S. F. McCormick, and L. Olson. Least-squares finite element methods and algebraic multigrid solvers for linear hyperbolic PDEs. *SIAM J. Sci. Comput.*, 26(1):31–54, 2004.
 - [12] H. De Sterck, T. A. Manteuffel, S. F. McCormick, and L. Olson. Numerical conservation properties of H(div)-conforming least-squares finite element methods for the burgers equation. *SIAM J. Sci. Comput.*, 26(5):1573–1597, 2005.
 - [13] L. Demkowicz and J. Gopalakrishnan. A class of discontinuous petrov–galerkin methods. part I: The transport equation. *Comput. Methods Appl. Mech. Eng.*, 199(23-24):1558–1572, 2010.
 - [14] O. Fuks and H. A. Tchelepi. Limitations of physics informed machine learning for nonlinear two-phase transport in porous media. *J. Mach. Learn. Modeling Comput.*, 1(1):19–37, 2020.
 - [15] D. Gottlieb and C.-W. Shu. On the Gibbs phenomenon and its resolution. *SIAM Review*, 39(4):644–668, 1997.
 - [16] J.-L. Guermond and M. Nazarov. A maximum-principle preserving C^0 finite element method for scalar conservation equations. *Comput. Methods Appl. Mech. Eng.*, 272:198–213, 2014.
 - [17] A. Harten, B. Engquist, S. Osher, and S. R. Chakravarty. Uniformly high order accurate essentially non-oscillatory schemes, III. In *Upwind and high-resolution schemes*, pages 218–290. Springer, 1987.
 - [18] J. S. Hesthaven. *Numerical Methods for Conservation Laws: From Analysis to Algorithms*. SIAM, 2017.
 - [19] J. S. Hesthaven and T. Warburton. *Nodal Discontinuous Galerkin Methods: Algorithms, Analysis, and Applications*. Springer Science & Business Media, 2007.
 - [20] P. Houston, J. A. Mackenzie, E. Süli, and G. Warnecke. A posteriori error analysis for numerical approximations of Friedrichs systems. *Numer. Math.*, 82(3):433–470, 1999.
 - [21] P. Houston, R. Rannacher, and E. Süli. A posteriori error analysis for stabilised finite element approximations of transport problems. *Comput. Methods Appl. Mech. Eng.*, 190(11-12):1483–1508, 2000.
 - [22] D. I. Ketcheson, R. J. LeVeque, and M. J. del Razo. *Riemann Problems and Jupyter Solutions*. SIAM, Philadelphia, 2020.
 - [23] D. P. Kingma and J. Ba. ADAM: A method for stochastic optimization. In *International Conference on Representation Learning, San Diego*, 2015; arXiv preprint arXiv:1412.6980.
 - [24] R. J. LeVeque. *Numerical Methods for Conservation Laws*. Birkhäuser, Boston, 1992.
 - [25] M. Liu and Z. Cai. Adaptive two-layer ReLU neural network: II. Ritz approximation to elliptic PDEs. *Comput. Math. Appl.*, 113:103–116, 2022.
 - [26] M. Liu, Z. Cai, and J. Chen. Adaptive two-layer ReLU neural network: I. best least-squares approximation. *Comput. Math. Appl.*, 113:34–44, 2022.
 - [27] S. Osher. Riemann solvers, the entropy condition, and difference approximations. *SIAM J. Numer. Anal.*, 21:217–235, 1984.
 - [28] M. Raissi, P. Perdikaris, and G. E. Karniadakis. Physics-informed neural networks: A deep learning framework for solving forward and inverse problems involving nonlinear partial differential equations. *J. Comput. Phys.*, 378:686–707, 2019.
 - [29] P. L. Roe. Approximate Riemann solvers, parameter vectors, and difference schemes. *J. Comput. Phys.*, 43(2):357–372, 1981.
 - [30] C.-W. Shu. Essentially non-oscillatory and weighted essentially non-oscillatory schemes for hyperbolic conservation laws. In *Advanced Numerical Approximation of Nonlinear Hyperbolic Equations*, pages 325–432. Springer, 1998.
 - [31] C.-W. Shu and S. Osher. Efficient implementation of essentially non-oscillatory shock-capturing schemes. *J. Comput. Phys.*, 77(2):439–471, 1988.
 - [32] J. Sirignano and K. Spiliopoulos. DGM: A deep learning algorithm for solving partial differential equations. *J. Comput. Phys.*, 375:1139–1364, 2018.
 - [33] J. W. Thomas. *Numerical Partial Differential Equations: Finite Difference Methods*, volume 22. Springer Science & Business Media, 2013.
 - [34] Z. Zhao, Y. Chen, and J. Qiu. A hybrid Hermite WENO scheme for hyperbolic conservation laws. *J. Comput. Phys.*, 405:109175, 2020.

7. Appendix. In the appendix, we provide the proofs of Lemmas 4.2 and 4.3. First, denote the integral and the mid-point/trapezoidal rule of a function φ over an interval $[0, \rho]$ by

$$I(\varphi) = \int_0^\rho \varphi(s) ds \quad \text{and} \quad Q(\varphi; 0, \rho, 1) = \begin{cases} \rho \varphi(\rho/2), & \text{midpoint,} \\ \frac{\rho}{2}(\varphi(0) + \varphi(\rho)), & \text{trapezoidal,} \end{cases}$$

respectively. Let $p, q \in (1, \infty]$ such that $1/p + 1/q = 1$. It is easy to show the following error bounds:

$$(7.1) \quad |I(\varphi) - Q(\varphi; 0, \rho, 1)| \leq \begin{cases} C \rho^{2+1/q} \|\varphi''\|_{L^p(0, \rho)}, & \text{if } \varphi \in C^2(0, \rho), \\ C \rho^{1+1/q} \|\varphi'\|_{L^p(0, \rho)}, & \text{if } \varphi \in C^1(0, \rho). \end{cases}$$

Proof of Lemma 4.2. We prove Lemma 4.2 only for the mid-point rule because it may be proved in a similar fashion for the trapezoidal rule. To this end, denote uniform partitions of the intervals $[x_i, x_{i+1}]$ and $[t_j, t_{j+1}]$ by

$$x_i = x_i^0 < x_i^1 < \dots < x_i^{\hat{m}} = x_{i+1}, \text{ and } t_j = t_j^0 < t_j^1 < \dots < t_j^{\hat{n}} = t_{j+1},$$

respectively, where $x_i^k = x_i + k\hat{h}$ and $t_j^k = t_j + k\hat{\delta}$; and $\hat{h} = h/\hat{m}$ and $\hat{\delta} = \delta/\hat{n}$ are the numerical integration mesh sizes. By (7.1), we have

$$\left| \int_{t_j^k}^{t_j^{k+1}} \sigma(x_i, x_{i+1}; t) dt - \hat{\delta} \sigma(x_i, x_{i+1}; t_j^{k+1/2}) \right| \leq C \hat{\delta}^{2+1/q} \|\sigma_{tt}(x_i, x_{i+1}; \cdot)\|_{L^p(t_j^k, t_j^{k+1})},$$

and

$$\left| \int_{x_i^k}^{x_i^{k+1}} u(x; t_j, t_{j+1}) dx - \hat{h} u(x_i^{k+1/2}; t_j, t_{j+1}) \right| \leq C \hat{h}^{2+1/q} \|u_{xx}(\cdot; t_j, t_{j+1})\|_{L^p(x_i^k, x_i^{k+1})},$$

which, together with (4.3), (4.4), and the triangle and the Hölder inequalities, implies

$$\begin{aligned} & |K_{ij}|^{1/q} \|\mathbf{div}_\tau \mathbf{f}(u) - \text{avg}_\tau \mathbf{div} \mathbf{f}(u)\|_{L^p(K_{ij})} = |K_{ij}| \left| \text{avg}_{K_{ij}} \mathbf{div} \mathbf{f}(u) - \mathbf{div}_\tau \mathbf{f}(u(\mathbf{m}_{ij})) \right| \\ & \leq C \left\{ h \hat{\delta}^{2+1/q} \sum_{k=0}^{\hat{n}-1} \|\sigma_{tt}(x_i, x_{i+1}; \cdot)\|_{L^p(t_j^k, t_j^{k+1})} + \delta \hat{h}^{2+1/q} \sum_{k=0}^{\hat{m}-1} \|u_{xx}(\cdot; t_j, t_{j+1})\|_{L^p(x_i^k, x_i^{k+1})} \right\} \\ & \leq C \left\{ h \hat{\delta}^{2+1/q} \hat{n}^{1/q} \|\sigma_{tt}(x_i, x_{i+1}; \cdot)\|_{L^p(t_j, t_{j+1})} + \delta \hat{h}^{2+1/q} \hat{m}^{1/q} \|u_{xx}(\cdot; t_j, t_{j+1})\|_{L^p(x_i, x_{i+1})} \right\}. \end{aligned}$$

This completes the proof of Lemma 4.2. \square

To prove Lemma 4.3, we need to estimate an error bound of numerical integration for piece-wise smooth and discontinuous integrant over interval $[0, \rho]$.

LEMMA 7.1. *For any $0 < \hat{\rho} < \rho/2$, assume that $\varphi \in C^1((0, \hat{\rho})) \cap C^1((\hat{\rho}, \rho))$ is a piece-wise C^1 function. Denote by $j_\varphi = |\varphi(\hat{\rho}^+) - \varphi(\hat{\rho}^-)|$ the jump of $\varphi(s)$ at $s = \hat{\rho}$. Then there exists a positive constant C such that*

$$(7.2) \quad \begin{aligned} |I(\varphi) - Q(\varphi; 0, \rho, 1)| & \leq C \rho^{1+1/q} \|\varphi'\|_{L^p((0, \rho) \setminus \{\hat{\rho}\})} + \begin{cases} \hat{\rho} j_\varphi, & \text{mid-point,} \\ \left| \frac{\rho}{2} - \hat{\rho} \right| j_\varphi, & \text{trapezoidal} \end{cases} \\ & \leq C \rho^{1+1/q} \|\varphi'\|_{L^p((0, \rho) \setminus \{\hat{\rho}\})} + \frac{\rho}{2} j_\varphi. \end{aligned}$$

Proof. Denote the linear interpolant of φ on the interval $[0, \rho]$ by $\varphi_1(s) = \varphi(0) \frac{\rho-s}{\rho} + \varphi(\rho) \frac{s}{\rho}$. For any $s \in (0, \hat{\rho})$, by the fact that $\varphi(0) - \varphi_1(0) = 0$, a standard argument on the error bound of interpolant yields that there exists a $\xi_- \in (0, \hat{\rho})$ such that

$$\varphi(s) - \varphi_1(s) = \varphi'(\xi_-)s - \frac{s}{\rho}(\varphi(\rho) - \varphi(0)),$$

which implies

$$\int_0^{\hat{\rho}} (\varphi(s) - \varphi_1(s)) ds = \int_0^{\hat{\rho}} \varphi'(\xi_-)s ds - \frac{\hat{\rho}^2}{2\rho} (\varphi(\rho) - \varphi(0)).$$

In a similar fashion, there exists a $\xi_+ \in (\hat{\rho}, \rho)$ such that

$$\int_{\hat{\rho}}^{\rho} (\varphi(s) - \varphi_1(s)) ds = \int_{\hat{\rho}}^{\rho} \varphi'(\xi_+)(s - \rho) ds + \frac{(\rho - \hat{\rho})^2}{2\rho} (\varphi(\rho) - \varphi(0)).$$

Combining the above inequalities and using the triangle and the Hölder inequalities give

$$\begin{aligned} |I(\varphi) - Q_t(\varphi)| &= \left| \int_0^{\hat{\rho}} \varphi'(\xi_-)s ds + \int_{\hat{\rho}}^{\rho} \varphi'(\xi_+)(s - \rho) ds + \frac{\rho - 2\hat{\rho}}{2} (\varphi(\rho) - \varphi(0)) \right| \\ &\leq \frac{1}{(1+q)^{1/q}} \rho^{1+1/q} (\|\varphi'\|_{L^p(0, \hat{\rho})} + \|\varphi'\|_{L^p(\hat{\rho}, \rho)}) + \left| \frac{\rho}{2} - \hat{\rho} \right| |\varphi(\rho) - \varphi(0)| \\ &\leq \frac{2^{1/q}}{(1+q)^{1/q}} \rho^{1+1/q} \|\varphi'\|_{L^p((0, \rho) \setminus \{\hat{\rho}\})} + \left| \frac{\rho}{2} - \hat{\rho} \right| |\varphi(\rho) - \varphi(0)|. \end{aligned}$$

It follows from the triangle and the Hölder inequalities that

$$\begin{aligned} |\varphi(\rho) - \varphi(0)| &\leq \left| \int_{\hat{\rho}}^{\rho} \varphi'(s) ds \right| + \left| \int_0^{\hat{\rho}} \varphi'(s) ds \right| + j_{\varphi} \\ &\leq \rho^{1/q} (\|\varphi'\|_{L^p(0, \hat{\rho})} + \|\varphi'\|_{L^p(\hat{\rho}, \rho)}) + j_{\varphi} \leq (2\rho)^{1/q} \|\varphi'\|_{L^p((0, \rho) \setminus \{\hat{\rho}\})} + j_{\varphi}. \end{aligned}$$

Now, the above two inequalities and the fact that $\left| \frac{\rho}{2} - \hat{\rho} \right| \leq \frac{\rho}{2}$ imply (7.2) for the trapezoidal rule.

To prove the validity of (7.2) for the mid-point rule, note that for any $s \in (0, \hat{\rho})$ we have

$$\begin{aligned} \varphi(s) - \varphi(\rho/2) &= \int_{\hat{\rho}}^s \varphi'(s) ds + \int_{\rho/2}^{\hat{\rho}} \varphi'(s) ds + \varphi(\hat{\rho}^-) - \varphi(\hat{\rho}^+) \\ &\leq (\hat{\rho} - s)^{1/q} \|\varphi'\|_{L^p(s, \hat{\rho})} + (\rho/2 - \hat{\rho})^{1/q} \|\varphi'\|_{L^p(\hat{\rho}, \rho/2)} + \varphi(\hat{\rho}^-) - \varphi(\hat{\rho}^+), \end{aligned}$$

which, together with the triangle inequality, implies

$$\left| \int_0^{\hat{\rho}} (\varphi(s) - \varphi(\rho/2)) ds \right| \leq \left(\frac{\rho}{2} \right)^{1+1/q} (\|\varphi'\|_{L^p(0, \hat{\rho})} + \|\varphi'\|_{L^p(\hat{\rho}, \rho/2)}) + \hat{\rho} j_{\varphi}.$$

Similarly, we have

$$\left| \int_{\hat{\rho}}^{\rho} (\varphi(s) - \varphi(\rho/2)) ds \right| \leq \frac{2q}{1+q} \left(\frac{\rho}{2} \right)^{1+1/q} \|\varphi'\|_{L^p(\hat{\rho}, \rho)}.$$

Now, (7.2) for the mid-point rule follows from the triangle inequality and the above two inequalities. This completes the proof of the lemma. \square

Now, we are ready to prove the validity of Lemma 4.3.

Proof of Lemma 4.3. By the assumption, the discontinuous interface Γ_{ij} intercepts two horizontal edges at (\hat{x}_i^l, t_l) for $l = j, j+1$. Without loss of generality, assume that $\hat{x}_i^j \in (x_i^{k_j}, x_i^{k_j+1})$ and $\hat{x}_i^{j+1} \in (x_i^{k_{j+1}}, x_i^{k_{j+1}+1})$ for some k_j and k_{j+1} in $\{0, 1, \dots, \hat{m}\}$. Let $\hat{I}_{ij} = (x_i^{k_j}, x_i^{k_j+1}) \cup (x_i^{k_{j+1}}, x_i^{k_{j+1}+1})$. The same proof of Lemma 4.2 leads to

$$\begin{aligned} & \|\mathbf{div}_\tau \mathbf{f}(u) - \text{avg}_\tau \mathbf{div} \mathbf{f}(u)\|_{L^p(K_{ij})} \\ & \leq C \left\{ \frac{h^{1/p} \delta^2}{\hat{n}^2} \|\sigma_{tt}(x_i, x_{i+1}; \cdot)\|_{L^p(t_j, t_{j+1})} + \frac{h^2 \delta^{1/p}}{\hat{m}^2} \|u_{xx}(\cdot; t_j, t_{j+1})\|_{L^p((x_i, x_{i+1}) \setminus \hat{I}_{ij})} \right\} \\ & \quad + \frac{\delta}{(h\delta)^{1/q}} \sum_{l=j}^{j+1} \left| \int_{x_i^{k_l}}^{x_i^{k_l+1}} u(x; t_j, t_{j+1}) dx - \hat{h} u(x_i^{k_l + \frac{1}{2}}; t_j, t_{j+1}) \right|, \end{aligned}$$

which, together with Lemma 7.1, implies

$$\begin{aligned} & \|\mathbf{div}_\tau \mathbf{f}(u) - \text{avg}_\tau \mathbf{div} \mathbf{f}(u)\|_{L^p(K_{ij})} \\ & \leq C \left(\frac{h^{1/p} \delta^2}{\hat{n}^2} + \frac{h^2 \delta^{1/p}}{\hat{m}^2} \right) + \frac{\hat{h} \delta}{(h\delta)^{1/q}} \sum_{l=j}^{j+1} \left\{ C \hat{h}^{1/q} \|u_x(\cdot; t_j, t_{j+1})\|_{L^p((x_i, x_{i+1}) \setminus \{\hat{x}_i^l\})} + \llbracket u(\hat{x}_i^l, t_l) \rrbracket \right\}. \end{aligned}$$

Now, (4.7) follows from $\hat{h} = h/\hat{m}$. This completes the proof of Lemma 4.3. \square